Journal of Pharmaceutical and Biomedical Analysis Open 1 (2023) 100011

Contents lists available at ScienceDirect

Journal of Pharmaceutical and Biomedical Analysis Open

journal homepage: www.journals.elsevier.com/journal-of-pharmaceutical-and-biomedical-analysis-open

Enantioseparation of new axially chiral carboxylic acids on polysaccharide-based chiral stationary phases under normal phase elution conditions

Barbara Sechi[a], Victor Mamane[b,*], Roberto Dallocchio[a], Alessandro Dessì[a], Sergio Cossu[c], Giorgi Jibuti[d], Paola Peluso[a,*]

[a] Istituto di Chimica Biomolecolare ICB-CNR, Sede secondaria di Sassari, Traversa La Crucca 3, Regione Baldinca, Li Punti, 07100 Sassari, Italy
[b] Institut de Chimie de Strasbourg, UMR CNRS 7177, Equipe LASYROC, 1 rue Blaise Pascal, 67008 Strasbourg Cedex, France
[c] Dipartimento di Scienze Molecolari e Nanosistemi DSMN, Università Ca' Foscari Venezia, Via Torino 155, I-30172 Mestre Venezia, Italy
[d] Institute of Physical and Analytical Chemistry, School of Exact and Natural Sciences, Tbilisi State University, Chavchavadze Ave 3, 0179 Tbilisi, Georgia

ARTICLE INFO

Keywords:
Atropisomers
Enantioseparation
High-performance liquid chromatography
Molecular modeling
Polysaccharide-based chiral stationary phases

ABSTRACT

In the last decade, the availability of new and versatile synthetic strategies for the preparation of substituted 4,4'-bipyridyl derivatives based on chemo- and regioselective functionalization of the 4,4'-bipyridine core has encouraged studies for exploring the bioactivity of these compounds in the fields of drug discovery and medicinal chemistry. In substituted 4,4'-bipyridines, chirality may emerge from restricted rotation induced by sterically hindered atoms or functional groups located around the 4,4'-biaryl bond (chiral axis). The first atropisomeric substituted 4,4'-bipyridine was prepared in 2008, and no asymmetric synthesis to produce pure atropisomers of chiral 4,4'-bipyridine derivatives has been available so far. Thus, in the last few years, our groups developed methods to separate atropisomers of a wide series of 4,4'-derivatives by high-performance liquid chromatography (HPLC) using polysaccharide-based chiral stationary phases (CSPs). In the frame of our interest in this field, we reported herein the synthesis of two new chiral carboxylic acids containing an axially chiral 4,4'-bipyridyl unit as source of chirality, and their HPLC enantioseparation on polysaccharide-based CSPs. In particular, the impact of analyte and CSP structures on the enantioseparation outcomes as well as mechanisms and noncovalent interactions underlying the enantioseparation were explored by using electrostatic potential analysis and molecular dynamics (MD) simulations.

1. Introduction

Classically, the 4,4'-bipyridyl unit has been mainly used as a divergent coordination linker between metals or metal complexes [1,2]. With this function, 4,4'-bipyridine and its derivatives have become a versatile molecular design element for the preparation of coordination polymers and metal–organic frameworks [1,3] towards applications in the fields of luminescence sensing [4], molecular electronics [5] and separation science [6,7]. Very recently, 4,4'-bipyridines showed to be versatile scaffolds for the preparation of self-assembled 2D-networks on highly oriented pyrolytic graphite, adopting structural motifs that are governed by the substituents [8]. Otherwise, applications of 4,4'-bipyridines in medicinal chemistry and drug discovery remain relatively unexplored [9–12] even though nitrogen heterocycles are very popular targets in these fields [13]. The reason for that likely relies on the fact that relatively few synthetic strategies leading to functionalized 4,4'-bipyridines were available in the distant past, and more efficient functionalization reactions have been developed only recently [14–19]. While developing efficient strategies for the syntheses of functionalized 4,4'-bipyridines [20,21], our groups found that 2,2'-disubstituted-3,3',5,5'-tetrachloro-4,4'-bipyridines (**1**) (Fig. 1) showed interesting capability to inhibit transthyretin fibrillation in vitro [20]. Some analogs belonging to the same series are currently under investigation showing remarkable antiproliferative activity toward melanoma cell lines [22].

It is worth mentioning that compounds of general structure **1** are chiral for atropisomerism by restricted rotation around the 4,4'-bond (chiral axis). In the last few decades, atropisomerism has been recognized as a relevant and versatile design element for drug discovery [23–25]. In particular, the separation of atropisomers at analytical and preparative level is important for determining possible enantioselective biological functions of the target compounds [26]. For six compounds

* Corresponding authors.
E-mail addresses: vmamane@unistra.fr (V. Mamane), paola.peluso@cnr.it (P. Peluso).

https://doi.org/10.1016/j.jpbao.2023.100011
Received 20 March 2023; Received in revised form 18 April 2023; Accepted 20 April 2023
2949-771X/© 2023 The Author(s). Published by Elsevier B.V. This is an open access article under the CC BY-NC-ND license (http://creativecommons.org/licenses/by-nc-nd/4.0/).

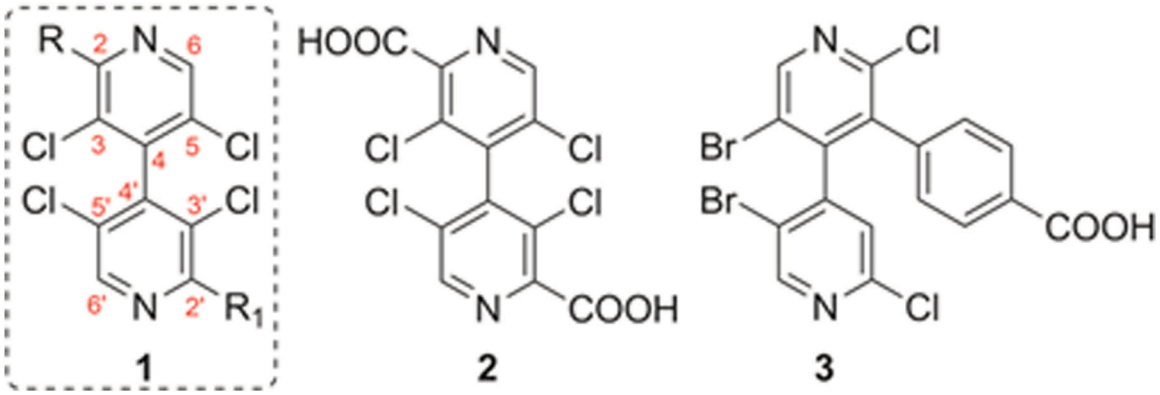

Fig. 1. Structures of chiral compounds **1**, 3,3',5,5'-tetrachloro-[4,4'-bipyridine]-2,2'-dicarboxylic acid (**2**) and 4-(5,5'-dibromo-2,2'-dichloro-[4,4'-bipyridin]-3-yl) benzoic acid (**3**).

of the series **1**, efficient methods for high-performance liquid chromatography (HPLC) enantioseparation on polysaccharide-based chiral stationary phases (CSPs) have been developed by our groups [22,27–30]. On the other hand, the first atropisomeric 4,4'-bipyridine was prepared in its racemic form in 2008 [31] and, likely due to the novelty of the field, no asymmetric synthesis for this class of chiral compounds has been available so far.

In general, chiral carboxylic acids are conveniently resolved by diastereomeric crystallization. It is the reason why, among the huge number of chiral analytes which can be enantioseparated on polysaccharide-based chiral columns [32,33], axially chiral carboxylic acids have attracted limited attention in chromatographic separation science. On the other hand, diastereomeric crystallization may be challenging if the carboxylic functionality is not close to the stereogenic element featuring the chiral molecule.

The first enantioseparation of an axially chiral carboxylic acid on a polysaccharide-based chiral selector dates back to 1978 [34], when Musso and co-authors reported the enantioseparation of the 6,6'-dinitro-2,2'-diphenic acid on potato starch. Overtime, attention was devoted to the enantioseparation of biphenyl [35,36] and binaphthyl [37,38] carboxylic acids on polysaccharide-based chiral columns, whereas methods to separate atropisomers of 4,4'-bipyridyl carboxylic acids were not reported so far.

In the frame of our interest toward chemistry of chiral 4,4'-bipyridines and their applications in medicinal chemistry [20,22], in the present study we explored the HPLC enantioseparation of two new axially chiral carboxylic acids (Fig. 1) on polysaccharide-based CSPs: *a*) the dicarboxylic acid **2** featuring again the 2,2'-disubstituted-3,3',5,5'-tetrachloro-4,4'-bipyridine scaffold, and *b*) compound **3** bearing a carboxyl group not directly bound to the 4,4'-bipyridine unit.

In this study, the impact of analyte and selector structures on the enantioseparation was also explored by using electrostatic potential (*V*) analysis, and the main noncovalent interactions underlying retention and selectivity were surveyed by molecular dynamics (MD). In this regard, it is worth noting that investigations on the enantioselective mechanisms underlying the enantioseparation of new chiral compounds may be of great interest to pave the way for new knowledge and information on the fine functioning of polysaccharide-based CSPs.

2. Materials and methods

2.1. General information, reagents and chemicals

Proton (^{1}H NMR) and carbon (^{13}C NMR) nuclear magnetic resonance spectra were recorded on a Bruker Avance III instrument operating at 500 MHz (Bruker Corporation, Billerica, MA, USA). The chemical shifts are given in parts per million (ppm) on the delta scale. The solvent peak was used as reference values for ^{1}H NMR ($CDCl_3$ = 7.26 ppm, CD_3OD = 3.31 ppm, CD_3COCD_3 = 2.05 ppm) and for ^{13}C NMR ($CDCl_3$ = 77.16 ppm, CD_3OD = 49.00 ppm, CD_3COCD_3 = 29.84 ppm). Data are presented as follows: chemical shift, multiplicity (s = singlet, d = doublet, t = triplet, q = quartet, dd = doublet of doublet), integration, and coupling constants (*J*/Hz). High-resolution mass spectra (HRMS) data were recorded on a micrOTOF spectrometer (Bruker Corporation, Billerica, MA, USA) equipped with an orthogonal electrospray interface (ESI). Analytical thin layer chromatography (TLC plates from Merck KGaA, Darmstadt, Germany) was carried out on silica gel 60 F254 plates with visualization by ultraviolet light. Reagents and solvents were purified using standard means. Dry acetonitrile was obtained by passing through activated alumina under a positive pressure of argon using GlassTechnology GTS100 devices. Dry triethylamine was distilled over CaH_2 and stored over KOH under an argon atmosphere. Anhydrous reactions were carried out in flame-dried glassware and under an argon atmosphere. All other chemicals were used as received.

2.2. Synthesis of 3,3',5,5'-tetrachloro-[4,4'-bipyridine]-2,2'-dicarboxylic acid (2) (Fig. 2A)

2.2.1. 3,3',5,5'-Tetrachloro-[4,4'-bipyridine]-2,2'-dicarbonitrile (4)

Bis-*N*-oxide **5** [21] (1.81 mmol, 590 mg) was dissolved in acetonitrile (7 mL) and triethylamine (1.7 mL). Trimethylsilylcyanide (10.86 mmol, 1.36 mL) was slowly added, and the mixture was refluxed at 100 °C for 24 h. After cooling to 0 °C, a solution of NaOH (5 M, 50 mL) was slowly added and the mixture was extracted with CH_2Cl_2 (3 × 60 mL). The combined organic phases were dried over $MgSO_4$, filtered and concentrated under vacuum. The crude compound was purified by chromatography on silica gel (pentane/ethyl acetate 7/3) to give **4** as a yellowish powder (458 mg, 73 %). ^{1}H NMR ($CDCl_3$, 500 MHz) δ 8.81 (s, 2 H) ppm; ^{13}C NMR ($CDCl_3$, 126 MHz) δ 149.3, 140.5, 135.0, 134.9, 132.5, 113.7 ppm. HRMS (ESI-TOF): *m/z* calcd. for $C_{12}H_3Cl_4N_4$ $[M+H]^+$: 342.9106, found: 342.9119.

2.2.2. 3,3',5,5'-Tetrachloro-[4,4'-bipyridine]-2,2'-dicarboxylic acid (2)

A resealable tube was charged with **4** (100 mg, 0.289 mmol) and a solution of NaOH (15 % in H_2O, 2.5 mL) was added. The tube was sealed and heated at 100 °C for 16 h. After cooling to room temperature, HCl 2 M was added until pH < 4 and the mixture was extracted with diethyl ether (4 × 10 mL). The combined organic phases were dried over Na_2SO_4. After filtration and concentration under vacuum, acid **2** was obtained as a white powder (105 mg, 95 %). ^{1}H NMR (CD_3OD, 500 MHz) δ 8.85 (s, 2H) ppm; ^{13}C NMR (CD_3OD, 126 MHz) δ 166.3, 149.5, 148.6, 143.2, 133.9, 130.3 ppm. HRMS (ESI-TOF): *m/z* calcd for $C_{12}H_3Cl_4N_2O_4$ $[M-H]^+$: 378.8852; found: 378.8861.

2.3. Synthesis of 4-(5,5'-dibromo-2,2'-dichloro-[4,4'-bipyridin] − 3-yl) benzoic acid **(3)** (Fig. 2B)

2.3.1. Ethyl 4-(5,5'-dibromo-2,2'-dichloro-[4,4'-bipyridin]-3-yl)benzoate **(6)**

A resealable tube was charged with **7** [16] (200 mg, 0.393 mmol), 4-ethoxycarbonylphenylboronic acid pinacol ester (109 mg, 0.393 mmol), sodium carbonate (88 mg, 0.786 mmol), THF (4 mL) and H_2O (1 mL). Argon was bubbled in the mixture for 10 min and $Pd(PPh_3)_4$ (22.7 mg, 0.02 mmol) was added. The tube was sealed and the mixture was heated at 80 °C for 12 h. After cooling, H_2O (10 mL) was added and the mixture extracted with CH_2Cl_2 (3 × 15 mL). The combined organic phases were dried over $MgSO_4$, filtered and concentrated under vacuum. The crude compound was purified by chromatography on silica gel (cyclohexane/ethyl acetate 7/1) to give **6** as a white solid (120 mg, 58 %). ^{1}H NMR ($CDCl_3$, 500 MHz) δ 8.70 (s, 1H), 8.43 (d, J = 0.5 Hz, 1H), 8.00 (dd, J = 8.0, 2.0 Hz, 1H), 7.85 (dd, J = 8.0, 2.0 Hz, 1H), 7.27 (dd, J = 8.0, 2.0 Hz, 1H), 7.19 (dd, J = 8.0, 2.0 Hz, 1H), 6.96 (d, J = 0.5 Hz, 1H), 4.36 (q, J = 7.0 Hz, 2H), 1.38 (t, J = 7.0 Hz, 3H) ppm; ^{13}C NMR ($CDCl_3$, 126 MHz) δ 165.8, 152.0, 151.0, 150.4, 150.2, 148.5, 147.2, 138.8, 136.1, 131.2, 130.0, 129.7, 129.5, 128.7, 125.2, 119.6, 119.4 ppm. HRMS (ESI-TOF): m/z calcd. for $C_{19}H_{13}Br_2Cl_2N_2O_2$ $[M+H]^+$: 528.8715, found: 528.8738.

2.3.2. 4-(5,5'-Dibromo-2,2'-dichloro-[4,4'-bipyridin]-3-yl)benzoic acid **(3)**

Ester **6** (20 mg, 0.0377 mmol) was dissolved in THF (3.8 mL). A solution of NaOH (4 mg, 0.094 mmol) in H_2O (3.8 mL) was added and the mixture was heated at 80 °C for 20 h. After cooling to room temperature, THF was removed under vacuum. To the residue in water was added HCl 2 M until pH = 1. The resulting white solid was filtrated and washed with water and pentane. The solid was dissolved in ethyl acetate and dried over $NaSO_4$. After filtration and concentration under vacuum, **3** was obtained as a white solid (15 mg, 79 %). ^{1}H NMR (CD_3COCD_3, 500 MHz) δ 8.82 (s, 1H), 8.55 (d, J = 0.5 Hz, 1H), 8.02 (dd, J = 8.0, 2.0 Hz, 1H), 7.99 (dd, J = 8.0, 2.0 Hz, 1H), 7.58 (d, J = 0.5 Hz, 1H), 7.52 (dd, J = 8.0, 2.0 Hz, 1H), 7.43 (dd, J = 8.0, 2.0 Hz, 1H) ppm; ^{13}C NMR (CD_3COCD_3, 126 MHz) δ 166.9, 152.7, 151.7, 150.8, 150.4, 149.7, 148.2, 140.1, 137.0, 131.9, 130.9, 130.5, 130.3, 129.6, 126.5, 120.4, 120.2 ppm. HRMS (ESI-TOF): m/z calcd. for $C_{17}H_9Br_2Cl_2N_2O_2$ $[M+H]^+$: 500.8402, found: 500.8424.

2.4. Chromatography

An Agilent Technologies (Waldbronn, Germany) 1100 Series HPLC system (high-pressure binary gradient system equipped with a diode-array detector operating at multiple wavelengths (220, 254, 280, 360 nm), a programmable autosampler with a 20 µl loop, and a thermostated column compartment) was employed for analytical separations. Data acquisition and analyses were carried out with Agilent Technologies ChemStation Version B.04.03 chromatographic data software. The UV absorbance is reported as milliabsorbance units (mAU). Lux Cellulose-1 [cellulose *tris*(3,5-dimethylphenylcarbamate)], Lux Cellulose-2 [cellulose *tris*(3-chloro-4-methylphenylcarbamate)], Lux Cellulose-3 [cellulose *tris*(4-methylphenylbenzoate)], Lux Cellulose-4 [cellulose *tris*(4-chloro-3-methylphenylcarbamate)], Lux i-Cellulose-5 [cellulose *tris*(3,5-dichlorophenylcarbamate)], Lux Amylose-1 and i-Amylose-1 [amylose *tris*(3,5-dimethylphenylcarbamate)], Lux Amylose-2 [amylose *tris*(5-chloro-2-methyl-phenylcarbamate)], and Lux i-Amylose-3 [amylose *tris*(3-chloro-5-methyl-phenylcarbamate)] were used as chiral columns (5 µm, 250 × 4.6 mm) (Phenomenex Inc., Torrance, CA, USA) (Table S1, Supplementary data). HPLC grade *n*-hexane, ethanol (EtOH), methanol (MeOH), 2-propanol (2-PrOH), and trifluoroacetic acid (TFA) were purchased from Sigma-Aldrich (Taufkirchen, Germany). Dead time (t_0) was measured by injection of tri-*tert*butylbenzene (Sigma-Aldrich) as a non-retained compound [39]. Analyses were performed in isocratic mode at 25 °C. The flow rate was set at 0.8 mL/min. For compounds **2** and **3**, the relative enantiomer elution order (EEO) was assigned by injecting pure enantiomers of unknown absolute configuration which were denoted as X_2 (X_3) and Y_2 (Y_3).

2.5. Computations

The 3D structures of compounds **2** and **3** were prepared using the build function, and model kits and tools provided by Spartan' 10 Version 1.1.0 (Wavefunction Inc., Irvine, CA, USA) [40] for building and editing organic molecules. Geometry optimization, energy calculations, and computation of electrostatic potential mapped on electron density isosurfaces (V_S) (0.002 au) and V_S extrema, maxima ($V_{S,max}$) and minima ($V_{S,min}$) values (kcal/mol) were performed at density functional theory (DFT) level (B3LYP, 6-311G*). V_S isosurface colors towards red depict negative V_S values, while colors towards blue depict positive V_S values and colors in between (orange, yellow, green) depict intermediate values of V_S. MD simulations were performed as described in the Supplementary data.

3. Results and discussion

3.1. Synthesis of the 4,4'-bipyridyl acid derivatives **2** and **3**

Formally, compound **2** is the dimer of 3-chloropicolinic acid. In this regard, it is worth mentioning that picolinic acid derivatives have attracted interest as ligands for the preparation of metal catalysts [41,42], and very recently chiral rhenium(I) picolinic acid complexes showed enantioselective inhibition of the SARS-CoV-2 main protease [43]. The synthesis of acid **2** (Fig. 2A) was performed starting from 4,4'-bipyridine **4**, obtained from bis-*N*-oxide **5** in good yield following a published procedure [21]. Thus, hydrolysis of the cyano groups of **4** under basic conditions furnished the targeted carboxylic acid **2** in high yield. The solubility of this carboxylic acid was sufficiently good in methanol to allow its unambiguous characterization by NMR spectroscopy. In particular, the typical chemical shift for the COOH group around 166 ppm was observed by ^{13}C NMR.

Carboxylic acid **3** was considered in our study in order to also evaluate the enantioseparability of a chiral 4,4'-bipyridine derivative bearing a *para*-linked benzoic acid unit, namely a COOH functionality not directly attached to the heteroaromatic unit. Acid **3** was obtained in two steps (Fig. 2B) from the pentahalogeno-bipyridine **7** [16]. In this case, a selective Suzuki cross-coupling reaction [44] on the more reactive C–I bond was first performed using 4-ethoxycarbonylphenylboronic acid pinacol ester to provide bipyridine **6** in moderate yield. The latter compound was hydrolyzed under basic conditions to generate carboxylic acid **3** in good yield. The COOH group of **3** was again attested by ^{13}C NMR spectroscopy, showing a chemical shift around 167 ppm. It is worth noting that the employed conditions for the hydrolysis did not cause the introduction of hydroxyl groups in 2,2'-positions of the bipyridine skeleton in place of the chlorine atoms, as confirmed by mass spectrometry.

3.2. Electrostatic potential analysis of the 4,4'-bipyridyl acid derivatives **2** and **3**

In order to explore the main recognition sites located on the molecular surfaces of compounds **2** and **3**, V_S values were calculated and compared (Table 1). Indeed, V is a real physical property, and the evaluation of its variations on a molecular electron density isosurface accounts for the shape of the molecule which is the sum of geometry and electronic distribution. On this basis, V analysis may give information on specific regions of the molecules, such as lone pairs and π-clouds. V (**r**) at each point **r** in the surrounding space of a molecule is created by each nucleus (first positive term) and electron (second

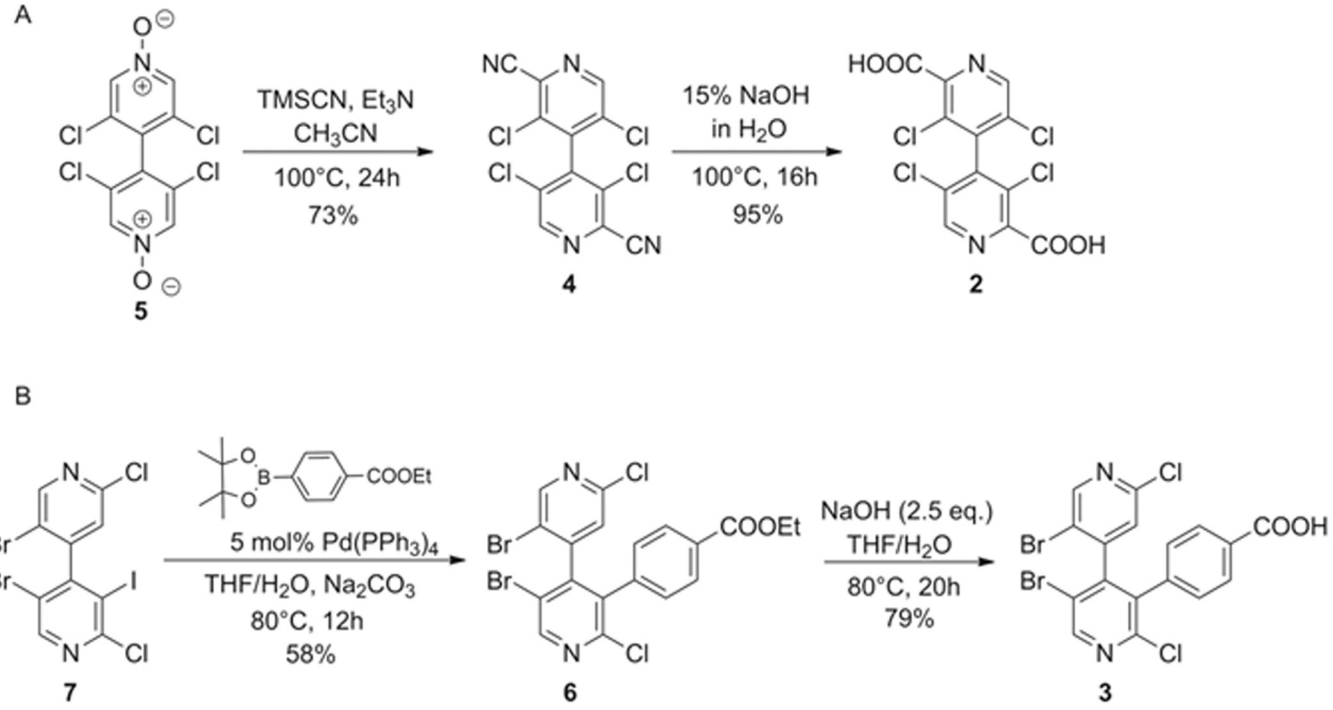

Fig. 2. Synthesis schemes of 3,3',5,5'-tetrachloro-[4,4'-bipyridine]-2,2'-dicarboxylic acid (**2**) and 4-(5,5'-dibromo-2,2'-dichloro-[4,4'-bipyridin]-3-yl)benzoic acid (**3**).

negative term) of the molecule and given by Eq. (1)

$$V(\mathrm{r}) = \sum_{A} \frac{Z_A}{R_A - \mathbf{r}} - \int \frac{\rho(\mathbf{r})d\mathbf{r}'}{|\mathbf{r}' - \mathbf{r}|} \quad (1)$$

where Z_A is the charge on nucleus A located at R_A, and $\rho(\mathbf{r})$ is the electron density function [45]. The sign of V may be positive or negative depending on the dominant contribution, which is positive and negative from nuclei and electrons. On this basis, electrophilic and nucleophilic properties may be associated with regions having positive and negative V, respectively.

Considering the linear relationships between pK_a and V_S values of acidic sites [46,47], compound **2** with the more positive $V_{s,max}$ value associated to the acidic proton appeared more acidic compared to compound **3** (68.81 vs 64.96 kcal/mol, Table 1). Moreover, considering trifluoroacetic acid, trichloroacetic acid, formic acid, benzoic acid, acetic acid, and picolinic acid as references for comparison, a good correlation was found between pK_a and calculated $V_{s,max}$ values for the acidic proton ($r^2 = 0.9456$) (Table S2, Supplementary data) allowing predicted pK_a values of 2.73 and 3.73 for **2** and **3**, respectively. The electron charge density on the carbonyl oxygen, expressed as negative $V_{s,min}$ value, was more negative for **2** (− 37.21 kcal/mol) compared to **3** (− 35.68 kcal/mol), revealing higher hydrogen bond (HB) acceptor ability for **2**. Analogously, the $V_{s,min}$ value on the oxygen bearing the acidic proton was more negative for **2** (− 21.84 kcal/mol) than for **3** (− 16.30 kcal/mol). Otherwise, the pyridyl nitrogen atoms of both compounds showed little differences as HB acceptors. Based on the overall description provided by the V analysis, higher retention was expected for compound **2** compared to **3** and lower selectivity due to *a*) the symmetry of the 3,3',5,5'-tetrachlorinated-4,4'-bipyridyl substructure, and *b*) the presence of strong HB sites at the 2,2'-position located far from the chiral axis. In previous studies, this feature proved to be detrimental for the enantioseparation of axially chiral compounds [36,48]. Moreover, the presence of the phenyl ring lent compound **3**

Table 1
Calculated V_S [kcal/mol] on a 0.002 au isosurface for 4,4'-bipyridines **2** and **3** (DFT/B3LYP/6-311G*).

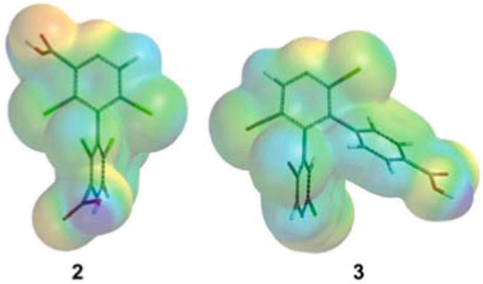

$V_{s,max}/V_{s,min}$ (Descriptor)	2	3
$V_{s,max}$ (COO*H*)	68.81	64.96
$V_{s,min}$ (C=*O*(OH))	-37.21	-35.68
$V_{s,min}$ (C=O(OH))	-21.84	-16.30
$V_{s,min}$ (N_{pyr})	-33.87	-33.37, - 34.08

(Log P = 5.73) a major hydrophobic feature compared to diacid **2** (Log P = 3.23).

3.3. Chromatographic screening

In this study, nine polysaccharide-based chiral columns were used to approach the enantioseparation of **2** and **3** under normal phase elution conditions (Table S1, Supplementary data): *a)* five coated (Lux Cellulose-1, Cellulose-2, Cellulose-3, and Cellulose-4) or immobilized (Lux i-Cellulose-5) cellulose-based columns, and *b)* four coated (Lux Amylose-1 and Amylose-2) or immobilized (Lux i-Amylose-1 and i-Amylose-3) amylose-based columns. Various *n*-hexane-based mixtures as mobile phases were tested by using 2-PrOH, EtOH, and MeOH as alcoholic modifiers, and TFA 0.1 % as acidic additive. Two reasons prompted us to focus on the use of *n*-hexane-based mobile phases: *a)* this type of mobile phase may be suitable for future preparative-scale separations, since removing organic solvents from the purified fractions is less energy-demanding compared to aqueous solutions, and *b)* modeling enantioseparation in a virtual normal-phase environment may provide a better picture of the noncovalent interactions underlying the contact between analyte enantiomers and polysaccharide-based selector.

3.3.1. Screening results for the chiral dicarboxylic acid **2**

As expected, the enantioseparation of the diacid **2** proved to be challenging, and in most cases very poor results were obtained and no remarkable improvement could be achieved by changing acidic additive and alcoholic modifier type and concentration, operative temperature and flow rate. When two peaks could be at least partially resolved, the EEO was X_2-Y_2 in all cases and no reversal of EEO was observed by changing polysaccharide-based column or elution conditions. Compound **2** was not eluted after 1 h with Cellulose-1, Cellulose-3, Cellulose-4, and Amylose-2 even by increasing the alcoholic modifier concentration in *n*-hexane up to 50%. A very large single peak was observed at 12.12 min by using the Cellulose-2 with *n*-hexane/2-PrOH 50:50 v/v as mobile phase. High retention and very broad peaks with remarkable tailing were obtained by using the i-Amylose-3 with *n*-hexane/2-PrOH 90:10 v/v (t_1 = 22.57 min; t_2 = 46.57 min). With this column a decrease of retention times could be achieved by changing 2-PrOH to EtOH, by increasing 2-PrOH concentration in *n*-hexane up to 50 %, and by increasing temperature to 45 °C. However, very low resolution was obtained in all mentioned cases. Compound **2** could be enantioseparated on the i-Cellulose-5 with acceptable retention times (t_1 = 16.687 min; t_2 = 21.252 min), but poor resolution and broad peaks were also obtained in this case. Acceptable results in terms of retention, selectivity and resolution were obtained with the i-Amylose-1, exclusively. The coated Amylose-1 provided similar results compared to the immobilized column, but an enhancement of peak tailing was observed in this case.

With the i-Amylose-1, the effect of increasing alcohol modifier concentration in *n*-hexane was evaluated in the range 10–50 % (v/v) by using 2-PrOH and EtOH as alcohols (Fig. 3 and Table S3, Supplementary data). Changing mobile phase composition from 90:10 (v/v) to 80:20 (v/v) (Fig. 3A,B) strongly impacted the retention times of both enantiomers, reducing elution times. Further increase of modifier concentration had lower effect on retention times that, anyway, decreased as the modifier concentration increased. For 2-PrOH, changing the concentration in the mobile phase from 10% to 20% increased the resolution (Fig. 3C), reducing peak tailing, whereas further addition of 2-PrOH was detrimental for the resolution. Otherwise, with EtOH, maximum resolution was obtained by using 10% alcohol concentration in the mobile phase, and further addition of alcohols reduced the resolution. On this basis, the best enantioseparation conditions for analyte **2** was obtained by using *n*-hexane/2-PrOH 80:20 (v/v) (α = 2.06, R_S = 4.7) (Fig. 3D) as mobile phase with the Lux i-Amylose-1.

The addition of MeOH to the mobile phase reduced retention times and selectivity, but no beneficial effect on the resolution was observed in this case.

3.3.2. Screening results for the chiral carboxylic acid **3**

Given that the best result for compound **2** was obtained on the Lux i-Amylose-1, the same screening conditions were applied to compound **3** for comparison. On this basis, the effect of increasing alcohol modifier concentration in *n*-hexane was evaluated in the range 10–50 % (v/v) by using 2-PrOH and EtOH as alcohols also for chiral acid **3** (Fig. S1 and Table S4, Supplementary data). For this compound, retention factors and resolution decreased as the content of the alcohol modifiers increased, and the best compromise between elution times and resolution was found by using *n*-hexane/EtOH 90:10 (v/v) as mobile phase (k_1 = 3.39, k_2 = 4.70, α = 1.39, R_S = 5.3) (Fig. S1D). For compound **3**, the resolution was higher than 1.5 in all cases, except that obtained with the mixture *n*-hexane/EtOH 50:50 (v/v) (R_S = 1.2). Overall, as expected, the enantioseparability of compound **3** appeared better than that of the diacid **2**, with better peak shape, lower retention times and higher resolution values. In all cases, the EEO was X_3-Y_3 and no mobile phase-dependent reversal of EEO was observed.

By using *n*-hexane/EtOH 90:10 (v/v) as mobile phase, the enantioseparation of chiral acid **3** was also explored on Cellulose-1, Cellulose-2, Cellulose-3, Cellulose-4, i-Cellulose-5, Amylose-1, Amylose-2, and i-Amylose-3 (Fig. 4 and Table S5, Supplementary data). In general, for compound **3** chlorinated cellulose columns provided higher selectivity compared to Cellulose-1, whereas Amylose-1 showed higher selectivity than the chlorinated amylose-based columns. Cellulose-2 furnished the best enantioseparation for acid **3** (k_1 = 2.36, k_2 = 2.87, α = 1.21, R_S = 2.6) among the cellulose-based chiral columns, whereas Amylose-1 provided the best selectivity (k_1 = 2.98, k_2 = 4.91, α = 1.65, R_S = 6.4) among the amylose-based columns. These results showed that *a)* the differences featuring cavities of the amylose and cellulose-based selectors impacted enantioselective recognition, and *b)* for the cellulose-based columns the change of the electron charge density on the carbamate moiety induced by the chlorine substituent impacted the enantioseparation at the molecular level in an opposite direction in comparison with the amylose-based columns. Even though Amylose-1 provided the highest selectivity value among the amylose-based column, i-Amylose-3 provided the best compromise between selectivity and elution time (k_1 = 2.71, k_2 = 3.74, α = 1.38, R_S = 4.1). It is worth noting that the absence of the N-H functionality in the cellulose benzoate-based chiral column (Lux Cellulose-3) increased retention and selectivity but not resolution compared to the other cellulose carbamate-based chiral selectors. The EEO was X_3-Y_3 with all chiral columns except for Amylose-2 that provided Y_3-X_3 as EEO, showing a pendant group-dependent reversal of the elution sequence compared to Amylose-1 (Fig. 5).

3.3.3. Comparison of the enantioseparations of **2** and **3**

Based on the structural features of the analyte under investigation, it could be hypothesized that the enantioseparation of diacid **2** is driven by the strong HB ability of the two COOH groups at the 2,2'-positions. For compound **3**, the enantioseparation outcome could be determined by the concurrent functions of the COOH group (HB site) and of the phenyl group (hydrophobic site). Thus, for diacid **2** increasing mobile phase polarity favored adsorption-desorption kinetics reducing peak tailing but, in parallel, polar interactions were strongly weakened or totally suppressed producing a decrease of both selectivity and resolution. On this basis, the efficacy of optimizing enantioseparation performances by tuning mobile phase polarity was very low for diacid **2**.

Otherwise, for compound **3**, increasing mobile phase polarity decreased HB strength and, in parallel, stabilized hydrophobic interactions. Thus, in this case enantioseparation could be more efficiently optimized by tuning mobile phase polarity. Coherently, on i-Amylose-1 compound **2** showed retention higher than **3** with mobile phase containing 10 % alcohol modifier due to its higher HB ability, whereas the opposite trend was observed with mobile phases containing higher percentages of modifier which weakened HBs and increased hydrophobic interactions. For instance, the addition of MeOH to the mobile

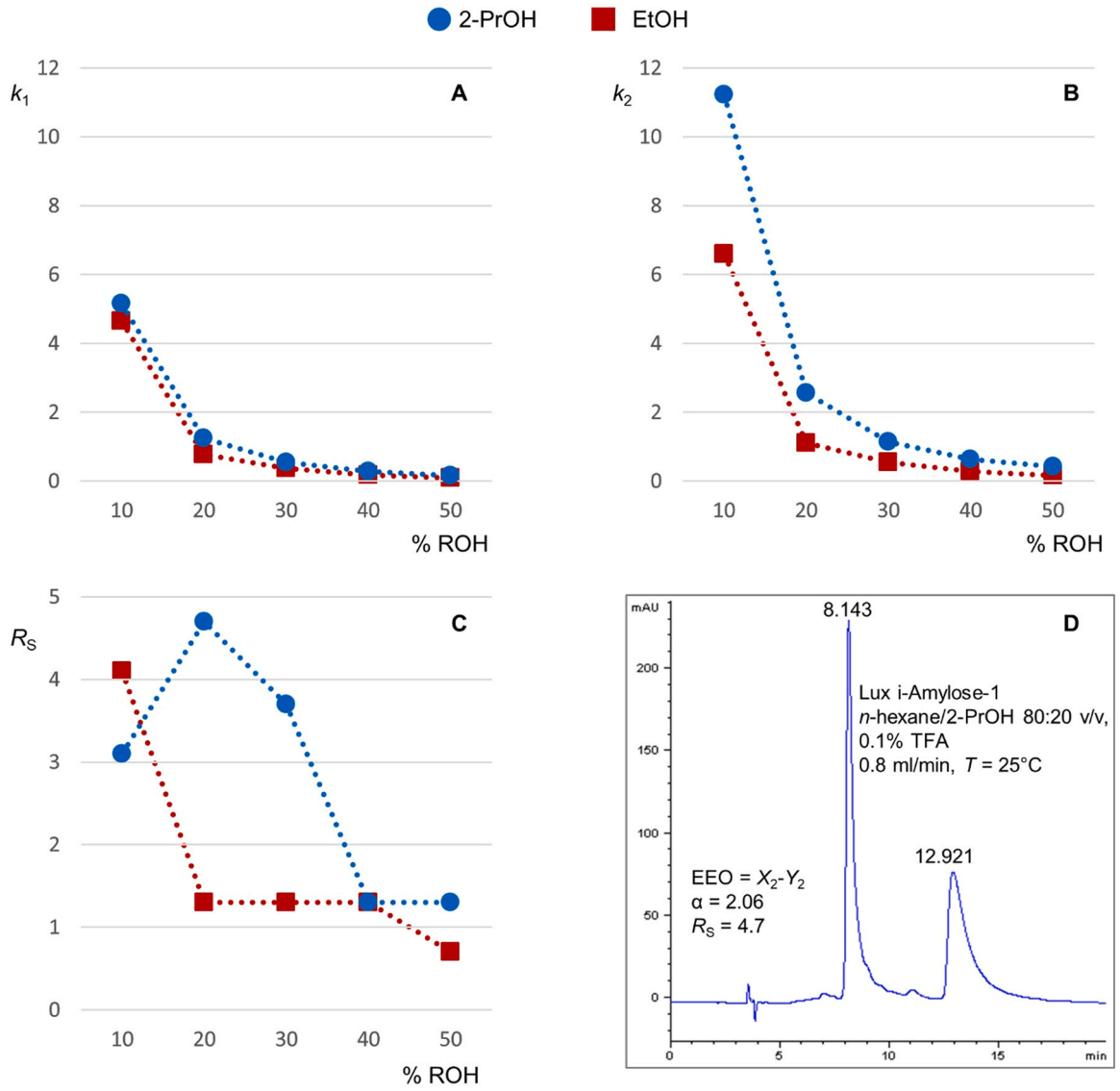

Fig. 3. Effect of mobile phase composition on k_1 (A), k_2 (B), and R_S (C) for analyte **2** on Lux i-Amylose-1 by using *n*-hexane/2-PrOH (●) and *n*-hexane/EtOH (■) mixtures as mobile phases (0.1 % TFA, flow rate = 0.8 mL/min, T = 25 °C); D: best enantioseparation conditions for analyte **2**.

phase reduced retention and appeared to be detrimental for selectivity and resolution in the case of **2**, whereas it also contributes to reduce elution time for **3** but maintaining good selectivity and resolution values (Fig. S2, Supplementary data).

Thus, for **3**, mobile phase polarity may be a useful tool to manage enantioseparation. For instance, the use of EtOH in place of 2-PrOH improved the enantioseparation of **3** with the Cellulose-1 and Cellulose-2 (Fig. S3A–D, Supplementary data). The opposite trend was observed with Amylose-1 (Fig. S3E,F).

3.4. MD simulations on amylose tris(3,5-dimethylphenylcarbamate) (ADMPC): diacid 2 vs monoacid 3

MD simulations were performed with the aim to explore the origin of the different enantioselective recognition of the 4,4'-bipyridyl acid derivatives **2** and **3**, as emerged from the experimental analysis. Thus, the enantioseparations of **2** and **3** on ADMPC, with *n*-hexane/2-PrOH 90:10 v/v as mobile phase, were considered and modeled as benchmark experimental data. The theoretical investigation based on MD simulations was performed by using the ADMPC nonamer as a virtual model of the polysaccharide-based selector. The 100 ns MD simulations were performed with the Generalized Amber Force Field (GAFF2) [49] in AMBER 18 [50] by using the mixture *n*-hexane/2-PrOH 90:10 as explicit virtual solvent in accord with the experimental conditions used in the chromatographic analyses. The total interaction energies calculated for (*M*)- and (*P*)-enantiomers of **2** and **3** in their complexes with the ADMPC nonamer are summarized in Table 2. The reported energies are Boltzmann weighted average values that were calculated from 5000 complexes obtained by snapshots taken every 20 ps from the 100 ns MD trajectories. The interaction energy (E_{int}) between the enantiomer and the selector was calculated based on the energies of the selector-enantiomer complex, the selector, and the enantiomer (Eq. (2)):

$$E_{int} = E_{total} - E_{enantiomer} - E_{polysaccharide-based\ selector} \quad (2)$$

where the E_{int} term is derived from the contributions of the van der Waals (vdW) and the electrostatic (el) interaction terms (Eq. (3)):

$$E_{int} = E_{el} + E_{vdW} \quad (3)$$

In Fig. 6, representative snapshots and noncovalent interactions from the simulated MD trajectories of the (*M*)- and (*P*)-enantiomers complexes

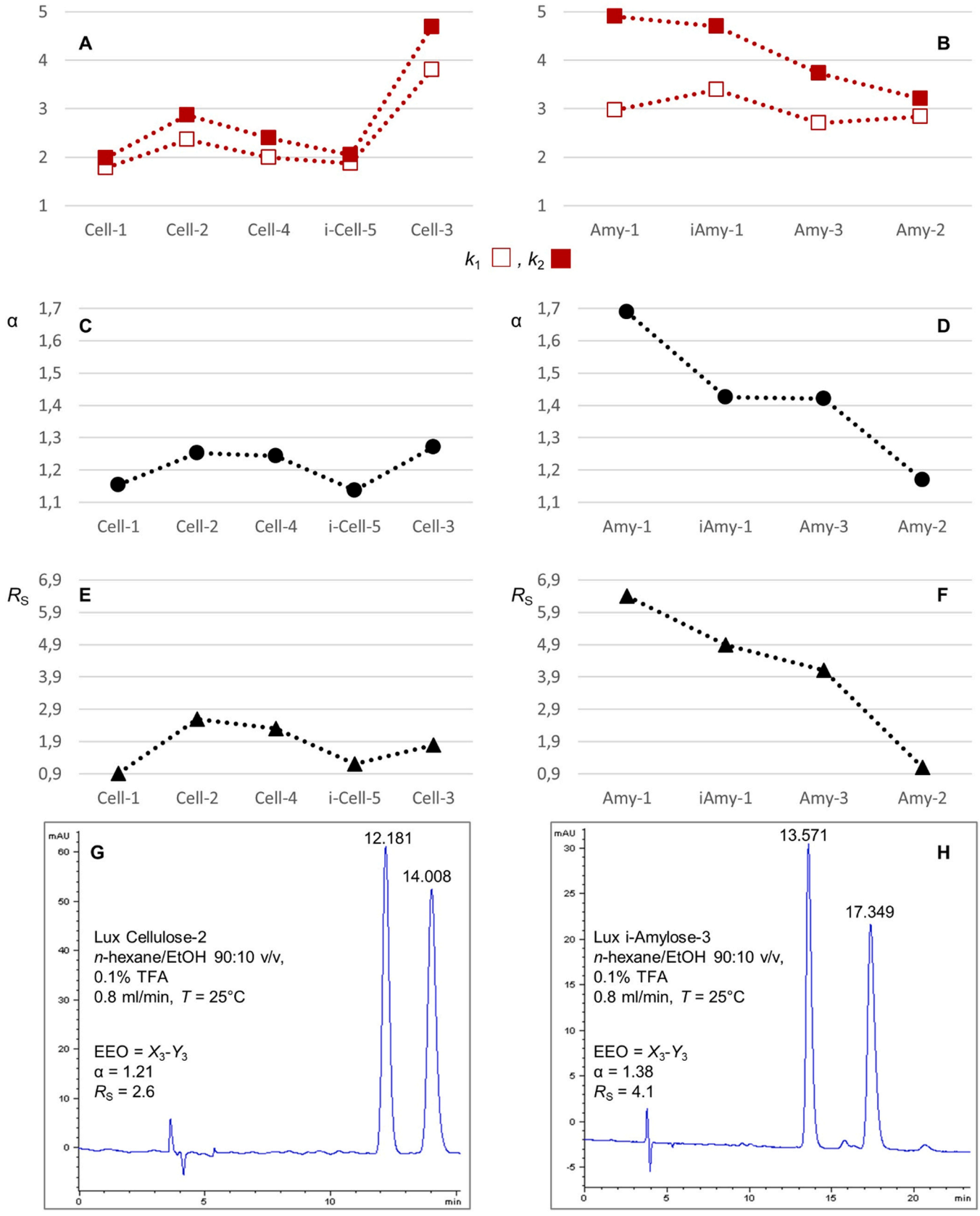

Fig. 4. Effect of CSP structure on k_1, k_2, α, and R_S for analyte **3** by using *n*-hexane/EtOH 90:10 (v/v) as mobile phase (0.1 % TFA, flow rate = 0.8 mL/min, T = 25 °C) on cellulose- (A, C, E) and amylose-based CSPs (B, D, F); best enantioseparation conditions for analyte **3** on Cellulose-2 (G) and i-Amylose-3 (H).

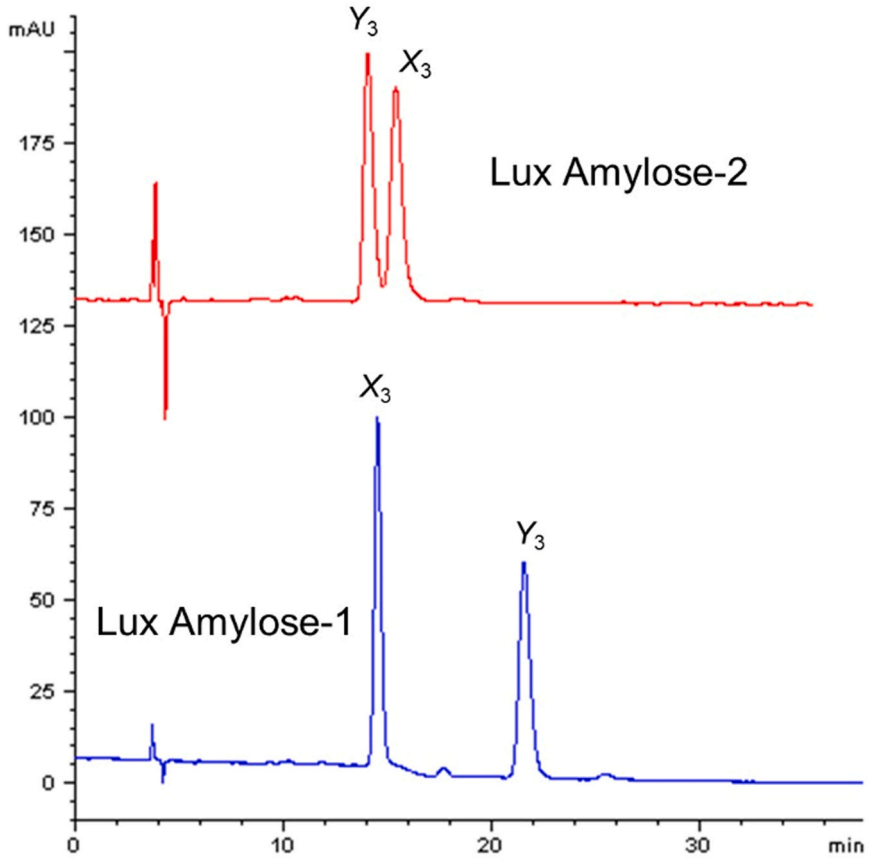

Fig. 5. Comparative enantioseparation of acid **3** on Lux Amylose-1 (EEO = X_3-Y_3) and Amylose-2 (EEO = Y_3-X_3): *n*-hexane/EtOH 90:10 (v/v), 0.1 % TFA, flow rate = 0.8 mL/min, T = 25 °C.

of **2** (A,B) and **3** (C,D) with ADMPC are depicted. In accordance with the experimental observations on the Lux i-Amylose-1 with *n*-hexane/2-PrOH 90:10 as mobile phase, MD analysis allowed reasonable conclusions to be drawn: *a)* at molecular level, the high retention of compound **2** could be ascribed to the strong HB ability of the two COOH groups at the 2,2'-positions (Fig. 6A,B); *b)* the limited enantiodiscrimination between the atropisomers of diacid **2** could be due to the symmetry of the HB system involving the COOH groups at the termini of the molecule and to the 3,3',5,5'-tetrachloro symmetric pattern around the 4,4'-bond as chiral axis; *c)* the enantioselective recognition of the atropisomers of acid **3** could be explained at molecular level with the occurrence for the most retained (*M*)-enantiomer of an enantioselective π-π interaction between the phenyl ring of the analyte bearing the COOH group and the 3,5-dimethylphenyl function of the selector (Fig. 6D). This interaction was not observed for the (*P*)-**3**-complex because the carboxyphenyl group of the analyte protruded outside the polymer groove (Fig. 6C).

Overall, the asymmetric noncovalent interaction patterns extracted by MD and underlying the diastereomeric complexes (*P*)-**3**- and (*M*)-**3**-

Table 2
Interaction energies (E_{int}) (kcal/mol) and component contributions (E_{el}, E_{vdW}) for the association of the (*P*)- and (*M*)-enantiomers of **2** and **3** with ADMPC, as derived from MD trajectories, and correlation with the experimental ln k[a] values.

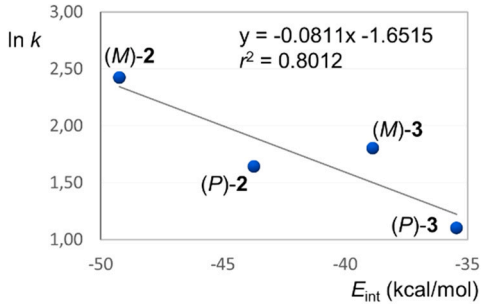

Compound	EEO_{calc}	E_{int}	E_{el}	E_{vdW}	ln k[a]
2	*P*	-43.72	-19.85	-23.87	1.64
	M	-49.23	-22.55	-26.68	2.42
3	*P*	-35.45	-8.64	-26.80	1.10
	M	-38.86	-10.79	-28.06	1.80

[a] Experimental retention factors (Lux i-Amylose-1, *n*-hexane/2-PrOH 90:10 v/v, see Tables S3 and S4, Supplementary data).

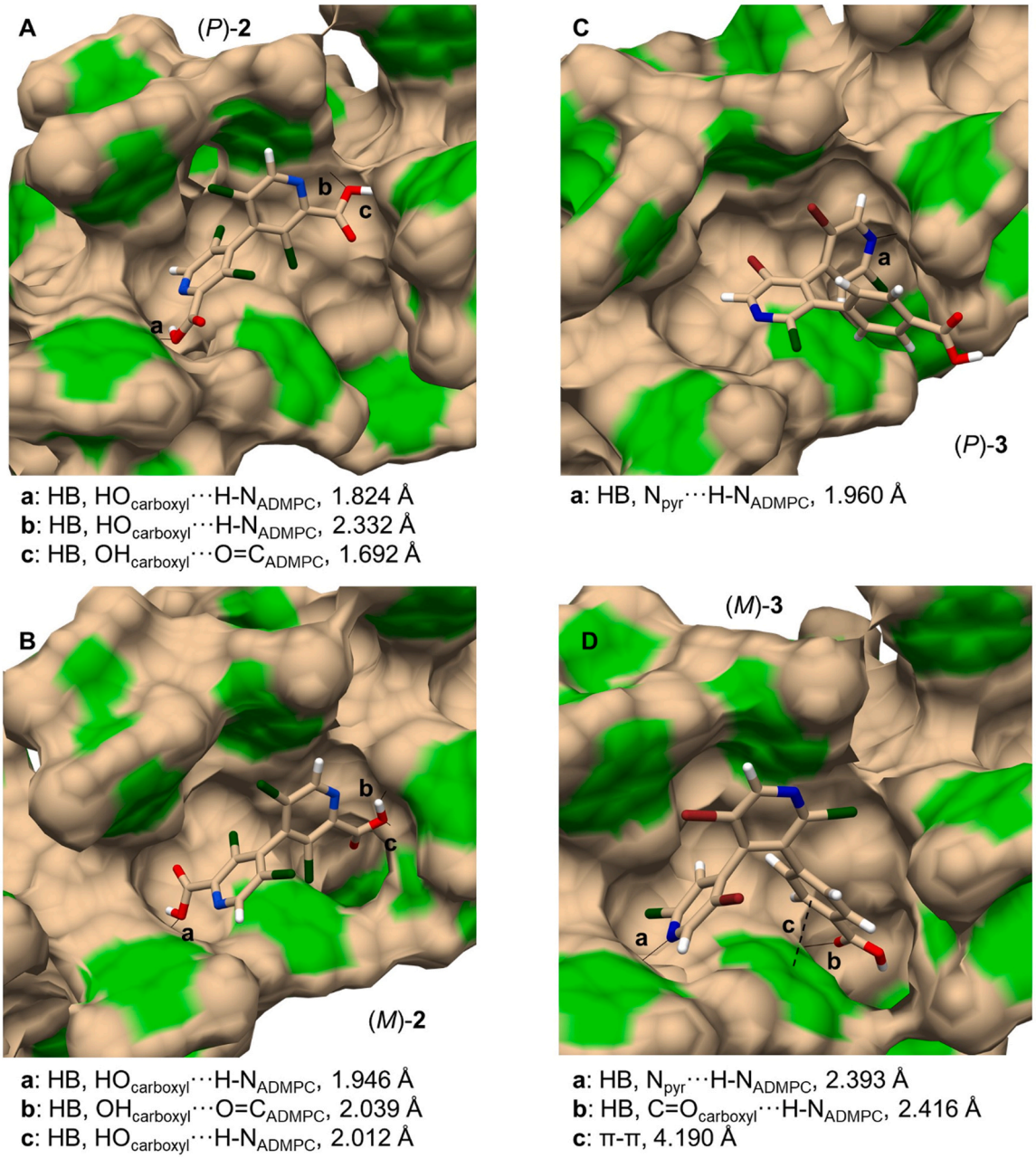

Fig. 6. Representative snapshots and noncovalent interactions from the simulated molecular dynamic (MD) trajectories of the complexes of (*P*)- and (*M*)-enantiomers of compounds **2** (A and B) and **3** (C and D) with amylose *tris*(3,5-dimethylphenylcarbamate) (ADMPC).

ADMPC may explain at the molecular level the higher enantioseparability of **3**. Otherwise, for **2**, the symmetry of the analyte as well as the symmetric noncovalent interaction patterns extracted by MD and underlying the diastereomeric complexes (*P*)-**2**- and (*M*)-**2**-ADMPC were both detrimental for the enantioselective recognition of the enantiomers.

Even though the absolute configuration assignment still needs to be confirmed experimentally, *a)* based on the noncovalent interaction patterns described above and *b)* by correlating the natural logarithm of the experimental retention factors with the E_{int} values extracted from the MD trajectory (r^2 = 0.8012), the absolute configuration for **2** and **3** enantiomers could be tentatively assigned as X_2, X_3 = *P* and Y_2, Y_3 = *M*. Given the (*M*)-enantiomers as the most retained for both analytes, a higher contribution of the E_{vdW} to the E_{int} was calculated for (*M*)-**3** (− 28.06/− 38.86, 72 %) compared to (*M*)-**2** (− 26.68/− 49.23, 54 %). Accordingly, the contribution of the E_{el} to the E_{int} was higher for (*M*)-**2** (− 22.55/− 49.23, 46 %) compared to (*M*)-**3** (− 10.79/− 38.86, 28 %).

4. Conclusions

In this study, we approached the enantioseparation of two new axially chiral carboxylic acids of potential interest for medicinal chemistry applications [20,22] by using nine polysaccharide-based chiral columns and *n*-hexane-based mixtures as mobile phases. The enantioseparation of diacid **2** proved to be more challenging compared to that of derivative **3** and, in most cases, the enantiomers of **2** were eluted with remarkable peak tailing or were not eluted after 60 min. Acceptable enantioseparation for this compound was obtained by using Lux i-Amylose-1, exclusively. The use of EtOH in place of 2-PrOH was shown to be beneficial for reducing elution times of **2** on the i-Amylose-1, but EtOH percentages higher than 10% provided resolution below

1.5. Indeed, for diacid **2**, increasing mobile phase polarity favoured adsorption-desorption kinetics reducing peak tailing but, in parallel, polar interactions were strongly weakened or totally suppressed producing a decrease of both selectivity and resolution. Otherwise, chiral acid **3** could be baseline enantioseparated on six chiral columns (Lux Cellulose-2, Cellulose-4, Cellulose-3, Amylose-1, i-Amylose-1, and i-Amylose-3) under the adopted conditions, with resolution factors in the range 1.8–6.4. For this compound, the best enantioseparation results were obtained with the Cellulose-2 and the i-Amylose-3 as a suitable compromise between short elution times and high selectivity and resolution. In the case of compound **3**, it is likely that the presence of the phenyl group between the COOH group and the 4,4'-bipyridyl unit contributed to decrease the acidity of the system, thus favouring hydrophobic and stacking interactions, even with mobile phase containing high percentages of alcoholic modifier. MD simulations were performed using a nonamer of ADMPC as virtual selector, and noncovalent interaction patterns underlying analyte-polymer complex formation were explored and identified as the possible reason of the diverse enantioseparation behaviors exhibited by compounds **2** and **3** on the ADMPC-based columns.

CRediT authorship contribution statement

Barbara Sechi: HPLC analysis, Data curation, Review & editing. **Victor Mamane:** Project administration, Syntheses, Funding acquisition, Writing – review & editing. **Roberto Dallocchio:** MD, Writing – review & editing. **Alessandro Dessì:** MD, Writing – review & editing. **Sergio Cossu:** Data curation, Writing – review & editing. **Giorgi Jibuti:** Data curation, Writing – review & editing. **Paola Peluso**: Conceptualization, Project administration, Data curation, Methodology, DFT calculations, Writing – original draft, Writing – review & editing.

Declaration of Competing Interest

The authors declare that they have no known competing financial interests or personal relationships that could have appeared to influence the work reported in this paper.

Acknowledgements

We thank CNR (Consiglio Nazionale delle Ricerche) (Grant no.: SAC.AD002.011) and SRNSFG (Shota Rustaveli National Science Foundation of Georgia) (Grant no.: CNR-22-259) for the Italy-Georgia Joint Bilateral Agreement, and the University of Strasbourg, the Centre National de la Recherche Scientifique (CNRS), and the French National Research Agency (Grant no.: ANR-21-CE07-0014) for financial support.

Appendix A. Supporting information

Supplementary data associated with this article can be found in the online version at doi:10.1016/j.jpbao.2023.100011.

References

[1] K. Biradha, M. Sarkar, L. Rajput, Crystal engineering of coordination polymers using 4,4'-bipyridine as a bond between transition metal atoms, Chem. Commun. (2006) 4169–4179, https://doi.org/10.1039/B606184B
[2] L. Armelao, D. Belli Dell'Amico, L. Bellucci, G. Bottaro, L. Labella, F. Marchetti, S. Samaritani, A convenient synthesis of highly luminescent lanthanide 1D-zigzag coordination chains based only on 4,4'-bipyridine as connector, Polyhedron 119 (2016) 371–376, https://doi.org/10.1016/j.poly.2016.09.009
[3] E. Aubert, M. Abboud, A. Doudouh, P. Durand, P. Peluso, A. Ligresti, B. Vigolo, S. Cossu, P. Pale, V. Mamane, Silver(I) coordination polymers with 3,3',5,5'-tetra-substituted 4,4'-bipyridine ligands: towards new porous chiral materials, RSC Adv. 7 (2017) 7358–7367, https://doi.org/10.1039/C6RA28197D
[4] S. Li, L. Lu, M. Zhu, S. Feng, F. Su, X. Zhao, Exploring the syntheses, structures, topologies, luminescence sensing and magnetism of Zn(II) and Mn(II) coordination polymers based on a semi-rigid tricarboxylate ligand, CrystEngComm 20 (2018) 5442–5456, https://doi.org/10.1039/C8CE00947C
[5] W. Zhao, W. Wang, J. Peng, T. Chen, B. Jin, S. Liu, W. Huang, Q. Zhao, Wrinkled two-dimensional ultrathin Cu(II)-porphyrin framework nanosheets hybridized with polypyrrole for flexible all-solid-state supercapacitors, Dalton Trans. 48 (2019) 9631–9638, https://doi.org/10.1039/C8DT05069D
[6] P. Peluso, V. Mamane, S. Cossu, Homochiral metal–organic frameworks and their application in chromatography enantioseparations, J. Chromatogr. A 1363 (2014) 11–26, https://doi.org/10.1016/j.chroma.2014.06.064
[7] J. Li, S. Chen, L. Jiang, D. Wu, Y. Li, Pore space partitioning of metal-organic framework for C_2H_x separation from methane, Inorg. Chem. 58 (2019) 5410–5413, https://doi.org/10.1021/acs.inorgchem.9b00550
[8] J. Richard, J. Joseph, C. Wang, A. Ciesielski, J. Weiss, P. Samorì, V. Mamane, J.A. Wytko, Functionalized 4,4'-bipyridines: synthesis and 2D organization on highly oriented pyrolytic graphite, J. Org. Chem. 86 (2021) 3356–3366, https://doi.org/10.1021/acs.joc.0c02708
[9] J. Stanek, G. Caravatti, H.-G. Capraro, P. Furet, H. Mett, P. Schneider, U. Regenass, *S*-Adenosylmethionine decarboxylase inhibitors: new aryl and heteroaryl analogues of methylglyoxal bis(guanylhydrazone), J. Med. Chem. 36 (1993) 46–54, https://doi.org/10.1021/jm00053a007
[10] B.-M. Swahn, Y. Xue, E. Arzel, E. Kallin, A. Magnus, N. Plobeck, J. Viklund, Design and synthesis of 2'-anilino-4,4'-bipyridines as selective inhibitors of c-Jun N-terminal kinase-3, Bioorg. Med. Chem. Lett. 16 (2006) 1397–1401, https://doi.org/10.1016/j.bmcl.2005.11.039
[11] S. Asaftei, D. Huskens, D. Schols, HIV-1 X4 activities of polycationic "viologen" based dendrimers by interaction with the chemokine receptor CXCR4: study of structure–activity relationship, J. Med. Chem. 55 (2012) 10405–10413, https://doi.org/10.1021/jm301337y
[12] R. Danac, I.I. Mangalagiu, Antimycobacterial activity of nitrogen heterocycles derivatives: bipyridine derivatives. Part III, Eur. J. Med. Chem. 74 (2014) 664–670, https://doi.org/10.1016/j.ejmech.2013.09.061
[13] L.D. Pennington, D.T. Moustakas, The necessary nitrogen atom: a versatile high-impact design element for multiparameter optimization, J. Med. Chem. 60 (2017) 3552–3579, https://doi.org/10.1021/acs.jmedchem.6b01807
[14] M. Abboud, V. Mamane, E. Aubert, C. Lecomte, Y. Fort, Synthesis of polyhalogenated 4,4'-bipyridines via a simple dimerization procedure, J. Org. Chem. 75 (2010) 3224–3231, https://doi.org/10.1021/jo100152e
[15] V. Mamane, E. Aubert, P. Peluso, S. Cossu, Synthesis, resolution, and absolute configuration of chiral 4,4'-bipyridines, J. Org. Chem. 77 (2012) 2579–2583, https://doi.org/10.1021/jo300286z
[16] V. Mamane, E. Aubert, P. Peluso, S. Cossu, Lithiation of prochiral 2,2'-dichloro-5,5'-dibromo-4,4'-bipyridine as a tool for the synthesis of chiral polyhalogenated 4,4'-bipyridines, J. Org. Chem. 78 (2013) 7683–7689, https://doi.org/10.1021/jo401255q
[17] V. Mamane, P. Peluso, E. Aubert, S. Cossu, P. Pale, Chiral hexahalogenated 4,4'-bipyridines, J. Org. Chem. 81 (2016) 4576–4587, https://doi.org/10.1021/acs.joc.6b00413
[18] R. Weiss, E. Aubert, P. Peluso, S. Cossu, P. Pale, V. Mamane, Chiral chalcogen bond donors based on the 4,4'-bipyridine scaffold, Molecules 24 (2019) 4484, https://doi.org/10.3390/molecules24244484
[19] B.T. Boyle, M.C. Hilton, A. McNally, Nonsymmetrical bis-azine biaryls from chloroazines: a strategy using phosphorus ligand-coupling, J. Am. Chem. Soc. 141 (2019) 15441–15449, https://doi.org/10.1021/jacs.9b08504
[20] A. Dessì, P. Peluso, R. Dallocchio, R. Weiss, G. Andreotti, M. Allocca, E. Aubert, P. Pale, V. Mamane, S. Cossu, Rational design, synthesis, characterization and evaluation of iodinated 4,4′-bipyridines as new transthyretin fibrillogenesis inhibitors, Molecules 25 (2020) 2213, https://doi.org/10.3390/molecules25092213
[21] E. Aubert, E. Wenger, P. Peluso, V. Mamane, Convenient access to functionalized non-symmetrical atropisomeric 4,4'-bipyridines, Compounds 1 (2021) 58–74, https://doi.org/10.3390/compounds1020006
[22] R. Dallocchio, A. Dessì, B. Sechi, B. Chankvetadze, S. Cossu, V. Mamane, E. Aubert, C. Rozzo, G. Palmieri, Y. Spissu, P. Peluso, Exploring interaction modes between polysaccharide-based selectors and biologically active 4,4'-bipyridines by experimental and computational analysis, J. Chromatogr. Open 2 (2022) 100030, https://doi.org/10.1016/j.jcoa.2022.100030
[23] J. Clayden, W.J. Moran, P.J. Edwards, S.R. LaPlante, The challenge of atropisomerism in drug discovery, Angew. Chem. Int. Ed. 48 (2009) 6398–6401, https://doi.org/10.1002/anie.200901719
[24] M. Basilaia, M.H. Chen, J. Secka, J.L. Gustafson, Atropisomerism in the pharmaceutically relevant realm, Acc. Chem. Res. 55 (2022) 2904–2919, https://doi.org/10.1021/acs.accounts.2c00500
[25] C. Donohoe, F.A. Schaberle, F.M.S. Rodrigues, N.P.F. Gonçalves, C.J. Kingsbury, M.M. Pereira, M.O. Senge, L.C. Gomes-da-Silva, L.G. Arnaut, Unraveling the pivotal role of atropisomerism for cellular internalization, J. Am. Chem. Soc. 144 (2022) 15252–15265, https://doi.org/10.1021/jacs.2c05844
[26] P. Peluso, V. Mamane, E. Aubert, S. Cossu, Recent trends and applications in liquid phase chromatography enantioseparation of atropisomers, Electrophoresis 38 (2017) 1830–1850, https://doi.org/10.1002/elps.201600502
[27] P. Peluso, V. Mamane, E. Aubert, A. Dessì, R. Dallocchio, A. Dore, P. Pale, S. Cossu, Insights into halogen bond-driven enantioseparations, J. Chromatogr. A 1467 (2016) 228–238, https://doi.org/10.1016/j.chroma.2016.06.007
[28] P. Peluso, V. Mamane, R. Dallocchio, A. Dessì, R. Villano, D. Sanna, E. Aubert, P. Pale, S. Cossu, Polysaccharide-based chiral stationary phases as halogen bond acceptors: a novel strategy for detection of stereoselective σ-hole bonds in solution, J. Sep. Sci. 41 (2018) 1247–1256, https://doi.org/10.1002/jssc.201701206
[29] P. Peluso, B. Sechi, G. Lai, A. Dessì, R. Dallocchio, S. Cossu, E. Aubert, R. Weiss, P. Pale, V. Mamane, B. Chankvetadze, Comparative enantioseparation of chiral 4,4'-

bipyridine derivatives on coated and immobilized amylose-based chiral stationary phases, J. Chromatogr. A 1625 (2020) 461303, https://doi.org/10.1016/j.chroma.2020.461303
[30] R. Dallocchio, B. Sechi, A. Dessì, B. Chankvetadze, S. Cossu, V. Mamane, R. Weiss, P. Pale, P. Peluso, Enantioseparations of polyhalogenated 4,4'-bipyridines on polysaccharide-based chiral stationary phases and molecular dynamics simulations of selector-selectand interactions, Electrophoresis 42 (2021) 1853–1863, https://doi.org/10.1002/elps.202100049
[31] A. Rang, M. Engeser, N.M. Maier, M. Nieger, W. Lindner, C.A. Schalley, Synthesis of axially chiral 4,4'-bipyridines and their remarkably selective self-assembly into chiral metallo-supramolecular squares, Chem. Eur. J. 14 (2008) 3855–3859, https://doi.org/10.1002/chem.200800113
[32] Y. Okamoto, E. Yashima, Polysaccharide derivatives for chromatographic separation of enantiomers, Angew. Chem. Int. Ed. 37 (1998) 1020–1043, https://doi.org/10.1002/(SICI)1521-3773(19980504)37:8<1020::AID-ANIE1020>3.0.CO;2-5
[33] B. Chankvetadze, Recent trends in preparation, investigation and application of polysaccharide-based chiral stationary phases for separation of enantiomers in high-performance liquid chromatography, Trends Anal. Chem. 122 (2020) 115709, https://doi.org/10.1016/j.trac.2019.115709
[34] H. Hess, G. Burger, H. Musso, Complete enantiomer separation by chromatography on potato starch, Angew. Chem. Int. Ed. Engl. 17 (1978) 612–614, https://doi.org/10.1002/anie.197806121
[35] Y. Liu, W. Lao, Y. Zhang, S. Jiang, L. Chen, Direct optical resolution of the enantiomers of axially chiral compounds by high-performance liquid chromatography on cellulose tris-(3,5-dimethylphenylcarbamate) stationary phase, Chromatographia 52 (2000) 190–194, https://doi.org/10.1007/BF02490455
[36] P. Peluso, D. Fabbri, M.A. Dettori, G. Delogu, V. Zambrano, S. Cossu, High-performance liquid chromatographic enantioseparation of atropisomeric biphenyls on seven chiral stationary phases, Curr. Org. Chem. 15 (2011) 1208–1229, https://doi.org/10.2174/138527211795203068
[37] L. Loukotková, M. Rambousková, Z. Bosáková, E. Tesařová, Cellulose tris(3,5-dimethylphenylcarbamate)-based chiral stationary phases as effective tools for enantioselective HPLC separation of structurally different disubstituted binaphthyls, Chirality 20 (2008) 900–909, https://doi.org/10.1002/chir.20585
[38] L. Loukotková, E. Tesařová, Z. Bosáková, P. Repko, D.W. Armstrong, Comparison of HPLC enantioseparation of substituted binaphthyls on CD-, polysaccharide- and synthetic polymer based chiral stationary phases, J. Sep. Sci. 33 (2010) 1244–1254, https://doi.org/10.1002/jssc.200900796
[39] H. Koller, K.–E. Rimböck, A. Mannschreck, High-pressure liquid chromatography on triacetylcellulose: characterization of a sorbent for the separation of enantiomers, J. Chromatogr. A 282 (1983) 89–94, https://doi.org/10.1016/S0021-9673(00)91594-2
[40] Y. Shao, L.F. Molnar, Y. Jung, J. Kussmann, C. Ochsenfeld, S.T. Brown, A.T.B. Gilbert, L.V. Slipchenko, S.V. Levchenko, D.P. O'Neil, R.A. Di Stasio Jr, R.C. Lochan, T. Wang, G.J.O. Beran, N.A. Besley, J.M. Herbert, C.Y. Lin, T. VanVoorhis, S.H. Chien, A. Sodt, R.P. Steele, V.A. Rassolov, P.E. Maslen, P.P. Korambath, R.D. Adamson, B. Austin, J. Baker, E.F.C. Byrd, H. Dachsel, R.J. Doerksen, A. Dreuw, B.D. Dunietz, A.D. Dutoi, T.R. Furlani, S.R. Gwaltney, A. Heyden, S. Hirata, C.–P. Hsu, G. Kedziora, R.Z. Khalliulin, P. Klunzinger, A.M. Lee, M.S. Lee, W.Z. Liang, I. Lotan, N. Nair, B. Peters, E.I. Proynov, P.A. Pieniazek, Y.M. Rhee, J. Ritchie, E. Rosta, C.D. Sherrill, A.C. Simmonett, J.E. Subotnik, H.L. Woodcock III, W. Zhang, A.T. Bell, A.K. Chakraborty, D.M. Chipman, F.J. Keil, A. Warshel, W.J. Hehre, H.F. Schaefer, J. Kong, A.I. Krylov, P.M.W. Gill, M. Head-Gordon, Advances in methods and algorithms in a modern quantum chemistry program package, Phys. Chem. Chem. Phys. 8 (2006) 3172–3191, https://doi.org/10.1039/B517914A
[41] S. Tanaka, Y. Suzuki, T. Kimura, M. Kitamura, A chiral picolinic acid ligand, Cl-Naph-PyCOOH, for CpRu-catalyzed dehydrative allylation: design, synthesis, and properties, Bull. Chem. Soc. Jpn. 92 (2019) 1707–1720, https://doi.org/10.1246/bcsj.20190134
[42] P. Wang, S. Cen, J. Gao, A. Shen, Z. Zhang, Novel axially chiral ligand-enabled copper-catalyzed asymmetric oxidative coupling of 2–naphthols for the synthesis of 6,6'-disubstituted BINOLs, Org. Lett. 24 (2022) 2321–2326, https://doi.org/10.1021/acs.orglett.2c00479
[43] J. Karges, M.A. Giardini, O. Blacque, B. Woodworth, J.L. Siqueira-Neto, S.M. Cohen, Enantioselective inhibition of the SARS-CoV-2 main protease with rhenium(I) picolinic acid complexes, Chem. Sci. 14 (2023) 711–720, https://doi.org/10.1039/D2SC05473F
[44] N. Miyaura, A. Suzuki, Palladium-catalyzed cross-coupling reactions of organoboron compounds, Chem. Rev. 95 (1995) 2457–2483, https://doi.org/10.1021/cr00039a007
[45] C. Gatti, A. Dessì, R. Dallocchio, V. Mamane, S. Cossu, R. Weiss, P. Pale, E. Aubert, P. Peluso, Factors impacting σ- and π-hole regions as revealed by the electrostatic potential and its source function reconstruction: the case of 4,4'-bipyridine derivatives, Molecules 25 (2020) 4409, https://doi.org/10.3390/molecules25194409
[46] P.W. Kenny, Hydrogen bonding, electrostatic potential, and molecular design, J. Chem. Inf. Model. 49 (2009) 1234–1244, https://doi.org/10.1021/ci9000234
[47] S. Liu, L.G. Pedersen, Estimation of molecular acidity via electrostatic potential at the nucleus and valence natural atomic orbitals, J. Phys. Chem. A 113 (2009) 3648–3655, https://doi.org/10.1021/jp811250r
[48] P. Peluso, V. Mamane, E. Aubert, S. Cossu, Insights into the impact of shape and electronic properties on the enantioseparation of polyhalogenated 4,4'-bipyridines on polysaccharide-type selectors. Evidence of stereoselective halogen bonding interactions, J. Chromatogr. A 1345 (2014) 182–192, https://doi.org/10.1016/j.chroma.2014.04.040
[49] J.A. Maier, C. Martinez, K. Kasavajhala, L. Wickstrom, K.E. Hauser, C. Simmerling, ff14SB: improving the accuracy of protein side chain and backbone parameters from ff99SB, J. Chem. Theory Comput. 11 (2015) 3696–3713, https://doi.org/10.1021/acs.jctc.5b00255
[50] D.A. Case, I.Y. Ben-Shalom, S.R. Brozell, D.S. Cerutti, T.E. Cheatham III, V.W.D. Cruzeiro, T.A. Darden, R.E. Duke, D. Ghoreishi, M.K. Gilson, H. Gohlke, A.W. Goetz, D. Greene, R. Harris, N. Homeyer, Y. Huang, S. Izadi, A. Kovalenko, T. Kurtzman, T.S. Lee, S. LeGrand, P. Li, C. Lin, J. Liu, T. Luchko, R. Luo, D.J. Mermelstein, K.M. Merz, Y. Miao, G. Monard, C. Nguyen, H. Nguyen, I. Omelyan, A. Onufriev, F. Pan, R. Qi, D.R. Roe, A. Roitberg, C. Sagui, S. Schott-Verdugo, J. Shen, C.L. Simmerling, J. Smith, R. Salomon-Ferrer, J. Swails, R.C. Walker, J. Wang, H. Wei, R.M. Wolf, X. Wu, L. Xiao, D.M. York, P.A. Kollman, Assisted Model Building with Energy Refinement (AMBER) v18 (Version 18), University of California, San Francisco, 2018〈https://ambermd.org/index.php〉.